C. R. Physique 12 (2011) 826–836

Contents lists available at ScienceDirect

Comptes Rendus Physique

www.sciencedirect.com

Nano- and micro-optomechanical systems / Nano- et micro-résonateurs optomécaniques

Towards the experimental demonstration of quantum radiation pressure noise

Pierre Verlot [a], Alexandros Tavernarakis [a], Chiara Molinelli [a], Aurélien Kuhn [a], Thomas Antoni [a], Slawomir Gras [a], Tristan Briant [a], Pierre-François Cohadon [a,*], Antoine Heidmann [a], Laurent Pinard [b], Christophe Michel [b], Raffaele Flaminio [b], Michaël Bahriz [a,c], Olivier Le Traon [c], Izo Abram [d], Alexios Beveratos [d], Rémy Braive [d], Isabelle Sagnes [d], Isabelle Robert-Philip [d]

[a] *Laboratoire Kastler Brossel, ENS-UPMC-CNRS, case 74, 4 place Jussieu, 75252 Paris cedex 05, France*
[b] *Laboratoire des matériaux avancés, CNRS/IN2P3, bâtiment Virgo, 7 avenue Pierre-de-Coubertin, 69622 Villeurbanne cedex, France*
[c] *ONERA, Physics Department, 29 avenue de la Division Leclerc, 92322 Châtillon cedex, France*
[d] *Laboratoire de photonique et de nanostructures, CNRS, route de Nozay, 91460 Marcoussis, France*

ARTICLE INFO

Article history:
Received 25 November 2010
Accepted 30 March 2011
Available online 16 June 2011

Keywords:
Quantum noise
Radiation pressure
Thermal noise
Gravitational-wave interferometers

Mots-clés :
Bruit quantique
Pression de radiation
Bruit thérmique
Interféromètres gravitationnels

ABSTRACT

Quantum radiation pressure noise has never been experimentally demonstrated, though it has been predicted for more than thirty years. It is, however, expected to limit the low-frequency sensitivity of second generation gravitational-wave interferometers. We have demonstrated classical radiation-pressure-induced correlations between two optical beams sent into the same high-finesse cavity with a moving mirror. Our two-beam scheme can be used to retrieve quantum noise embedded in an overwhelming classical noise, and has applications both in high-sensitivity measurements and in quantum optics.

RÉSUMÉ

Bien que prévu depuis plus de trente ans, le bruit quantique de pression de radiation n'a jamais été mis en évidence expérimentalement. On s'attend néanmoins à ce qu'il limite la sensibilité à basse fréquence des interféromètres gravitationnels de seconde génération. Nous avons mis en évidence des corrélations classiques induites par la pression de radiation entre deux faisceaux envoyés dans la même cavité de grande finesse dont un miroir est mobile. Notre dispositif à deux faisceaux permet de retrouver le bruit quantique même lorsque le bruit classique est prédominant, et a des applications dans les domaines des mesures de grande sensibilité et de l'optique quantique.

1. Introduction

Quantum radiation pressure noise (QRPN) has been studied for more than thirty years [1,2], in particular in the framework of gravitational wave detection [3,4]. Radiation pressure builds up correlations between intensity fluctuations and mirror displacements inside the optical interferometer and enforces quantum limits to the sensitivity of large-scale interferometers [1,2,5]. Overcoming such limits was a major motivation for the squeezing experiments [6–8] performed since then.

* Corresponding author.
E-mail address: cohadon@spectro.jussieu.fr (P.-F. Cohadon).

1631-0705/$ – see front matter
doi:10.1016/j.crhy.2011.03.008

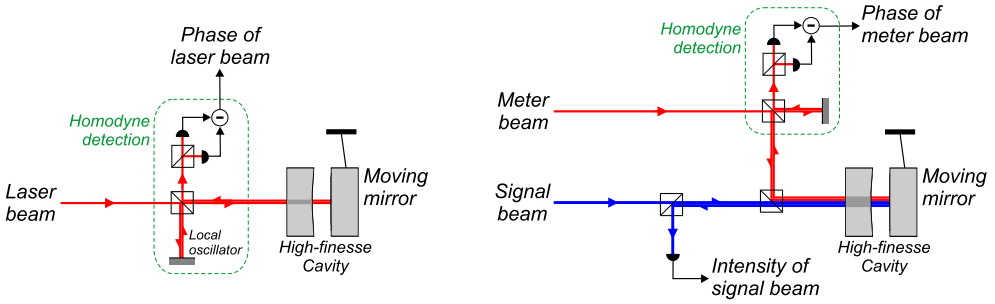

Fig. 1. Two possible experimental setups to demonstrate quantum radiation pressure noise (QRPN). (Left) One laser beam is sent into a moving mirror cavity. The reflected field is monitored by a homodyne detection and reproduces the mirror motion. QRPN appears as a displacement noise spectrum scaling as the intracavity power P. (Right) Two-beam setup: both an intense signal beam and a weaker meter beam are sent into the cavity. Intensity fluctuations of the signal beam are imprinted by radiation pressure onto the position fluctuations of the moving mirror, and onto the phase fluctuations of the meter beam. The two reflected beams then display intensity–phase correlations, retrieved with both a photodiode and a homodyne detection.

Meanwhile, a number of table-top experimental setups have been designed in order to demonstrate radiation pressure effects with smaller scale optomechanical resonators. However, the pioneering experiments [9–11] had to deal with a low optomechanical coupling and more recent ones [12–17] mainly focused on the possible demonstration of the quantum ground state of a mechanical resonator [18–20], so that up to now, QRPN still hasn't been demonstrated, the only exception being a related optical back-action heating of ultracold atoms trapped in a high-finesse cavity [21].

A conceptually simple experiment to demonstrate QRPN is to simply monitor the displacement noise spectrum of a moving mirror probed by laser light in an optical cavity. At (very) high power, such a noise spectrum should only be related to QRPN, with a characteristic linear dependence with the power P^{in} of the incident laser beam. Such a technique is currently being developed in medium-size experiments [22], typically performed with small-size moving mirrors embedded within large-scale optical interferometers, taking advantage of the technical background in both suspensions and vacuum systems of the gravitational-wave experimental groups involved.

As such an experiment involves a combination of low temperature, high mechanical quality factor and a very high optical power for QRPN to prevail over thermal displacement noise, we report in this work a novel two-beam technique [23,24] in order to demonstrate optomechanical correlations close to the quantum level. As a proof-of-principle, classical optomechanical correlations have been measured with a tiny classical intensity modulation that mimics QRPN. A closely related experiment is also underway with a membrane optical cavity setup [25].

In Section 2, we review the experimental challenge set by such a QRPN-demonstration experiment. We then proceed to present in Section 3 the principle of our experiment and related experimental results in Section 4. In Section 5, we review the way to extend our results to the quantum domain in order to demonstrate QRPN. Section 6 is dedicated to a review of the different approaches towards the ultimate optomechanical resonator currently under study at Laboratoire Kastler Brossel.

2. QRPN: an experimental challenge

For a lossless single-ended optical cavity at resonance (see Fig. 1, left), neglecting the cavity bandwidth effects, the phase fluctuations $\delta\varphi^{\text{out}}$ of the reflected field are:

$$\delta\varphi^{\text{out}} = \delta\varphi^{\text{in}} + \frac{8\mathcal{F}}{\lambda}(\delta x_{\text{cl}} + \delta x_{\text{rad}}) \tag{1}$$

where $\mathcal{F}$ is the cavity finesse, λ the laser wavelength, $\delta\varphi^{\text{in}}$ the (quantum) phase fluctuations of the incoming field, δx_{cl} the classical displacement fluctuations of the moving mirror inserted in the cavity (thermal noise, low-frequency vibrations, etc.) and δx_{rad} its position fluctuations induced by the (possibly quantum) fluctuations of the intracavity intensity.

To monitor radiation pressure effects down to the quantum level, one obviously has to enhance the optomechanical coupling with a high-finesse cavity ($\mathcal{F} \gg 1$): this makes the measurement noise $\delta\varphi^{\text{in}}$ negligible, provided the mirror displacements are large enough, which is easily met at or close to a mechanical resonance frequency. Monitoring the displacement noise spectrum through the phase of the reflected field (see Fig. 1, left) is then sufficient to demonstrate QRPN as long as the position fluctuations δx_{rad} induced by the quantum intensity fluctuations of the signal beam are the dominant noise source. This requires to lower the thermal fluctuations δx_{T} of the moving mirror. For a harmonic oscillator of mass M, resonance frequency $\Omega_{\text{M}}/2\pi$, and mechanical quality factor Q, the corresponding ratio between the radiation pressure and thermal noise spectra can be written [23,24]:

$$\frac{S_x^{\text{rad}}}{S_x^{\text{T}}} \simeq 2.3\left(\frac{\mathcal{F}}{300\,000}\right)^2\left(\frac{800\text{ nm}}{\lambda}\right)\left(\frac{P^{\text{in}}}{1\text{ mW}}\right)\times\left(\frac{1\text{ mg}}{M}\right)\left(\frac{Q}{10^6}\right)\left(\frac{1\text{ MHz}}{\Omega_{\text{M}}/2\pi}\right)\times\left(\frac{1\text{ K}}{T_{\text{m}}}\right) \tag{2}$$

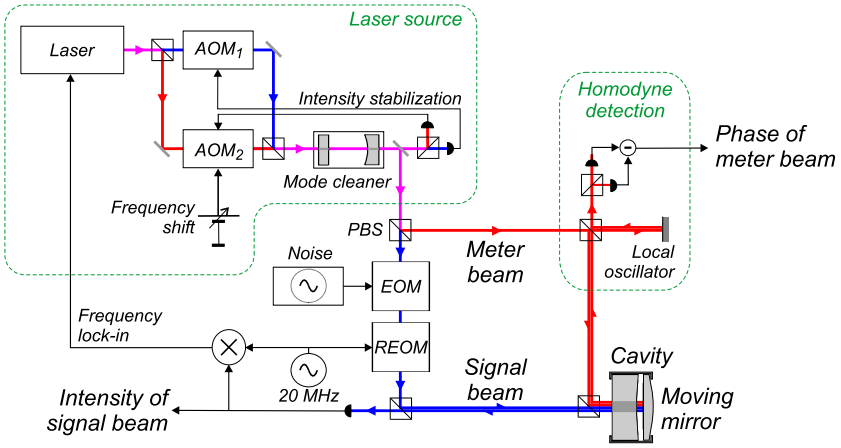

Fig. 2. Experimental setup. The laser beam is split in two independent beams by a polarizing beamsplitter (PBS). A resonant electro-optical modulator (REOM) is used to lock the laser onto the optical resonance via a Pound–Drever–Hall technique. Acousto-optic modulators (AOM_1 and AOM_2) are used to stabilize the intensities of both beams after their spatial filtering by the mode cleaner cavity. A second EOM modulates the intensity of the signal beam to mimic quantum radiation pressure noise. Intensity fluctuations of the reflected signal beam are monitored with a photodiode, as are the phase fluctuations of the meter beam with a quantum-limited homodyne detection. For simplicity, most polarizing elements are not shown.

where T_m is the mirror environment temperature and P^{in} the incident power of the laser beam. The stated values have all already been achieved independently in various state-of-the-art optomechanical systems [12–17,26,27], but combining the favourable mechanical behaviour of NEMS [26] with a very high optical finesse [27] is an even greater experimental challenge. However, a number of experiments are currently carried out in order to reach a regime where the ratio (2) is larger than one [22].

3. Two-beam setup

In order to demonstrate QRPN, we have developed an alternative approach. Two beams are sent into the same moving mirror cavity (see Fig. 1, right): the intensity fluctuations of the first, intense, signal beam drive the mirror into motion by radiation pressure, whereas the resulting position fluctuations are monitored through the phase of the second, weaker, meter beam.

Indeed, neglecting optical losses and irrelevant noises such as the quantum fluctuations of the meter beam, we have the following input–output relations for the fluctuations of the various fields involved, at a given frequency Ω [24]:

$$\delta I_s^{\text{out}}[\Omega] = \frac{1+i\omega}{1-i\omega}\delta I_s^{\text{in}}[\Omega] \tag{3}$$

$$\delta\varphi_m^{\text{out}}[\Omega] = \frac{8\mathcal{F}}{\lambda(1-i\omega)}\left(\delta x_{\text{T}}[\Omega] + \delta x_{\text{rad}}[\Omega]\right) \tag{4}$$

with straightforward definitions for the fluctuations, and $\omega = \Omega/\Omega_{\text{cav}}$ is the reduced frequency (Ω_{cav} is the cavity bandwidth). The radiation pressure noise δx_{rad} is related to the incident signal intensity fluctuations by:

$$\delta x_{\text{rad}}[\Omega] = \frac{8\mathcal{F}}{\lambda(1-i\omega)}\hbar\chi[\Omega]\delta I_s^{\text{in}}[\Omega] \tag{5}$$

where $\chi[\Omega]$ is the mechanical susceptibility of the moving mirror. The reflected signal intensity noise δI_s^{out} reproduces the incident fluctuations δI_s^{in}, with only a global phase shift, whereas the reflected meter phase $\delta\varphi_m^{\text{out}}$ reproduces the same incident signal intensity δI_s^{in} via the mirror motion (Eqs. (4) and (5)): the intensity–phase correlations observable between the two reflected beams therefore provide a direct measurement of the optomechanical correlations in the regime where radiation pressure noise prevails over thermal noise.

4. Experimental implementation and results

4.1. Experimental setup

The signal and meter beams are cross-polarized beams, emitted by the same Titane–Sapphire laser working at 810 nm. As the cavity is birefringent, two independent acousto-optic modulators (AOM_1 and AOM_2 in Fig. 2) detune the two beams so that they both match the cavity resonance. The overall resonance is controlled by locking the laser frequency via a Pound–Drever–Hall technique. A mode cleaner ensures the quality of the spatial profile of both beams, while their intensities are stabilized by servo-loops which drive the amplitude control of the AOMs.

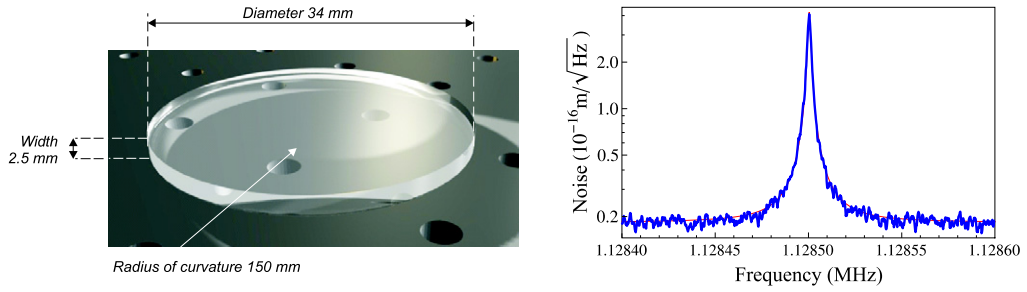

Fig. 3. Fused silica plano-convex mirrors used as optomechanical resonators. (Left) Geometrical characteristics of the resonator. (Right) Thermal noise spectrum of the fundamental mechanical mode, with a mechanical quality factor $Q = 750\,000$.

The moving mirror cavity is a single-ended optical cavity, with a 1-inch fused silica cylindrical input mirror and a moving mirror based on a fused silica resonator (see Section 4.2) as end mirror. Concerning its optical characteristics, the low roughness of the silica substrates allows for ultra low-loss optical coatings. We have obtained a cavity finesse $\mathcal{F} = 330\,000$, mainly limited by the 20 ppm transmission of the input mirror, which is crucial as additional losses would lower the quantum correlations between the intracavity and output fields. The cavity is only 0.33 mm long in order to keep a sufficient cavity bandwidth ($\Omega_{\text{cav}}/2\pi = 700$ kHz). It also prevents laser frequency noise from limiting the displacement sensitivity.

The phase fluctuations $\delta\varphi_m^{\text{out}}$ of the reflected meter beam are monitored by a homodyne detection. For an incident power of 500 μW, one gets a shot-noise-limited displacement sensitivity at the 10^{-20} m/$\sqrt{\text{Hz}}$ level for frequencies above 200 kHz. This makes quantum phase noise completely negligible in the vicinity of mechanical resonances. Intensity fluctuations δI_s^{out} of the reflected signal beam are monitored by a high-efficiency photodiode. Optical rejection of the double-beam system is higher than 35 dB, in such a way that phase fluctuations of the meter beam are insulated from the intensity fluctuations of the signal beam: observable effects of the signal beam are then necessarily induced by intracavity radiation pressure.

As our current optomechanical system is expected to have a ratio $S_x^{\text{rad}}/S_x^{\text{T}}$ around 10^{-3} [Eq. (2)], we have first tested our setup with an additional classical intensity noise which mimics QRPN [27,28]: the signal beam (150 μW) is intensity-modulated with an electro-optic modulator (EOM in Fig. 2) before entering the cavity to produce a classical intracavity radiation pressure noise. The driving noise has a typical bandwidth of a few hundreds of Hz, larger than any bandwidth used in the correlations acquisition process: it can therefore be considered as a white noise. The center frequency Ω_{c} of the noise is not necessarily at the mechanical resonance frequency Ω_{M}: working at resonance ($\Omega_{\text{c}} = \Omega_{\text{M}}$) indeed amplifies the radiation pressure and thermal displacements by a factor up to the quality factor Q, but the strong amplitude and phase dependencies of the mechanical response across the resonance has to be taken into account in order to analyze the resulting mirror motion. Note that the ratio (2) does not depend on the frequency, at least as long as mechanical losses can be considered constant. Furthermore, we will see in Section 5 that operating at the resonance actually presents some drawbacks when aiming at demonstrating QRPN. We therefore focus in the following on experimental results obtained at a lower frequency, with $\Omega_{\text{c}}/2\pi = 1.123$ MHz, about 600 mechanical linewidths below the resonance frequency ($\Omega_{\text{M}}/2\pi = 1.125$ MHz and $Q > 500\,000$).

All fluctuations are monitored through their quadratures [30]. In the case of the signal beam intensity for instance, its incident fluctuations δI_s^{in} are defined with respect to Ω_{c} by:

$$\delta I_s^{\text{in}}(t) = X_{I_s}^{\text{in}}(t)\cos(\Omega_{\text{c}}t) + Y_{I_s}^{\text{in}}(t)\sin(\Omega_{\text{c}}t) \tag{6}$$

where $X_{I_s}^{\text{in}}(t)$ and $Y_{I_s}^{\text{in}}(t)$ are slowly-varying noises. These two quadrature noises are randomly generated by a computer and loaded into a dual-channel waveform generator (Tektronix AFG3022B) in order to produce the two amplitude-modulated cosine and sine functions oscillating at frequency Ω_{c} in Eq. (6). These signals are then summed to drive the EOM, with a resulting radiation pressure noise δx_{rad} up to 5 times larger than the mirror thermal noise δx_{T} ($S_x^{\text{rad}}/S_x^{\text{T}} \lesssim 25$). Two spectrum analyzers Agilent MXA directly extract the quadratures of the reflected signal intensity ($X_{I_s}^{\text{out}}(t)$, $Y_{I_s}^{\text{out}}(t)$) and meter phase ($X_{\varphi_m}^{\text{out}}(t)$, $Y_{\varphi_m}^{\text{out}}(t)$) with an analysis bandwith of 400 Hz. Temporal evolution of the quadratures are acquired over a span time of 200 ms, equal to the scan time of the random amplitude-modulation pattern.

4.2. Fused silica mirrors as optomechanical resonators

For this specific experiment, according to Eq. (2), we have favoured optical characteristics and used a cm-size fused silica moving mirror. As such a mirror takes advantage of the amount of work performed in the framework of gravitational-wave detection to decrease optical and mechanical losses, it provides both a very high optical finesse and mechanical quality factor, at the expense of a mass in the mg range.

The actual moving mirror, used as the end mirror of the high-finesse cavity, is a plano-convex 34-mm diameter and 2.55-mm thick mirror (see Fig. 3), which displays Gaussian internal vibration modes [29]. We work at frequencies close to a

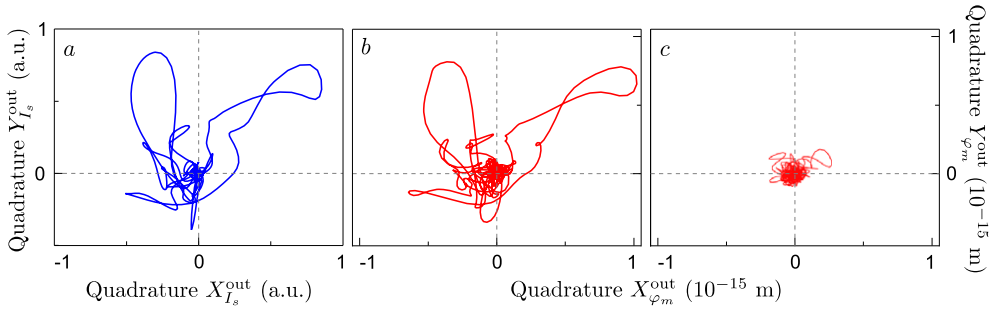

Fig. 4. Phase-space trajectories of the intensity noise of the reflected signal beam (a) and the phase noise of the meter beam, in the case $S_x^{\rm rad}/S_x^{\rm T} \simeq 25$ (b) and $S_x^{\rm rad}/S_x^{\rm T} \simeq 1$ (c). The phase noise is calibrated as displacements of the moving mirror. The main features of the intensity random walk can be seen on the phase noise as well when $S_x^{\rm rad}/S_x^{\rm T} \gg 1$, giving a first evidence for optomechanical correlations, whereas phase noise mainly depicts thermal noise for smaller $S_x^{\rm rad}/S_x^{\rm T}$ ratios.

mechanical resonance with the following optomechanical characteristics, deduced from the thermal noise spectrum at room temperature: $\Omega_{\rm M}/2\pi = 1.125$ MHz, $M \simeq 50$ mg (strongly dependent on the beam spot location over the resonator surface), and $Q = 750\,000$ in vacuum. This Gaussian mode is actually well confined around the central axis of the plano-convex structure, and the effective mass of the mode is thus much smaller than the total mass of the mirror, on the order of 5 g. This also prevents clamping losses at the edge of the mirror that may otherwise decrease the mechanical quality factor.

4.3. Results in phase space

Fig. 4 presents the observed phase-space trajectories of the reflected signal intensity and meter phase, drawn as the temporal evolution of the quadratures in their respective planes: clear correlations are evident between the intensity noise of the signal beam (left) and the meter phase noise in the case $S_x^{\rm rad} \gg S_x^{\rm T}$ (center). Radiation pressure noise is however still superimposed to the thermal noise $\delta x_{\rm T}$, which explains the small glitches observed between the two trajectories. Note the typical level of displacement, at the 10^{-15} m level.

Beyond this striking visual demonstration of the correlations, these can be quantified by computing the correlation coefficient $\mathcal{C}_{I_s,\varphi_m}$ defined from both trajectories:

$$\mathcal{C}_{I_s,\varphi_m} = \frac{\langle \delta I_s^{\rm out\star}\, \delta\varphi_m^{\rm out}\rangle}{\Delta I_s^{\rm out}\, \Delta\varphi_m^{\rm out}} \tag{7}$$

where the brackets $\langle\cdots\rangle$ stand for a temporal average and Δ represents the corresponding standard deviation. In the case $S_x^{\rm rad}/S_x^{\rm T} \simeq 25$, we obtain a correlation coefficient $|\mathcal{C}_{I_s,\varphi_m}|^2 \simeq 0.96$, in excellent agreement with the expected value $(1 + S_x^{\rm T}/S_x^{\rm rad})^{-1}$ deduced from Eqs. (3) to (5) [24].

In the $S_x^{\rm rad} \lesssim S_x^{\rm T}$ case, the reflected meter phase fluctuations $\delta\varphi_m^{\rm out}$ are mainly related to random thermal noise and the differences between both trajectories are not just glitches but far more severe (see Fig. 4, right). The correlation coefficient computed from a single experimental run has little meaning as its value strongly fluctuates from one run to the other.

4.4. Averaging to retrieve low correlation coefficients

It is however well known that when using a correlation technique, getting a signal out of the noise is mainly a matter of time. Indeed, our experimental setup enables to demonstrate optomechanical correlations even in the $S_x^{\rm rad} \ll S_x^{\rm T}$ case. The technique is emphasized on Fig. 5, which presents several runs performed with the same random intensity noise pattern (with $S_x^{\rm rad}/S_x^{\rm T} \simeq 0.03$) and the subsequent averaging of 500 runs, together with a close-up in phase space.

Averaging over these 500 runs, the thermal noise contribution – though overwhelming at the single-run level – eventually averages to zero while the radiation pressure term – though negligible over a single run – does not. Consequently, averaging the individual trajectories allows to recover the intensity noise pattern, on a scale much smaller than the single-shot thermal noise scale. The resulting averaged correlation coefficient also eventually tends to its small but non-zero expected value $(1 + S_x^{\rm T}/S_x^{\rm rad})^{-1} \simeq 0.03$, with a statistical uncertainty at least 10-times smaller (2.5×10^{-3} for 500 averages) [24].

5. Towards QRPN

The optomechanical correlations demonstrated so far are still at the classical level but QRPN in our system would correspond to $S_x^{\rm rad}/S_x^{\rm T} \simeq 10^{-3}$ for a temperature of 1 K. Further averaging once working at low temperature should then be sufficient to retrieve the corresponding quantum correlations and hence demonstrate radiation pressure noise. In this section, we estimate the required averaging time and discuss the implications of the cavity losses upon the laser/cavity frequency stability requirements.

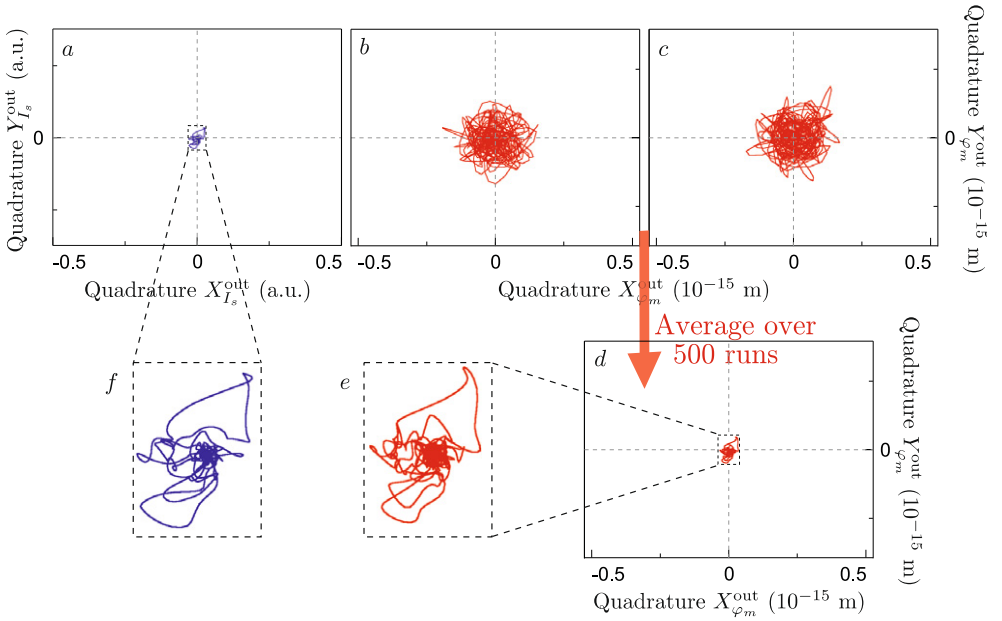

Fig. 5. Proof of principle of the ability of the two-beam setup to retrieve quantum optomechanical correlations even in the $S_x^{\rm rad}/S_x^{\rm T} \ll 1$ limit. Phase-space trajectory of the intensity noise of the signal beam (*a*) now corresponds to a ratio $S_x^{\rm rad}/S_x^{\rm T} = 0.03$, and the resulting phase noise of the meter beam for different experimental runs (*b*) and (*c*) is blurred by thermal noise. The initial intensity noise pattern is retrieved by the average of 500 similar experimental runs (*d*), and close-ups (*e*) and (*f*).

5.1. Constraints on averaging

When the motion is dominated by the thermal noise ($S_x^{\rm rad} \ll S_x^{\rm T}$), the correlation coefficient appears as the sum of two contributions $\mathcal{C}_{I_s,\varphi_m} \simeq \mathcal{C}_{\rm rad} + \mathcal{C}_{\rm T}$ deduced from Eqs. (4) and (7):

$$\mathcal{C}_{\rm rad} = \frac{\langle \delta I_s^{\rm out\star}\, \delta x_{\rm rad}\rangle}{\Delta I_s^{\rm out} \Delta x_{\rm T}}, \qquad \mathcal{C}_{\rm T} = \frac{\langle \delta I_s^{\rm out\star}\, \delta x_{\rm T}\rangle}{\Delta I_s^{\rm out} \Delta x_{\rm T}} \tag{8}$$

The first term represents the quantum optomechanical correlations induced by radiation pressure, whereas the second term vanishes as the intensity fluctuations are uncorrelated with the thermal noise. Both terms are effectively normalized to $\Delta x \simeq \Delta x_T$. Using Eqs. (3) and (5), the correlation coefficient then reduces to $|\mathcal{C}_{I_s,\varphi_m}|^2 \simeq S_x^{\rm rad}/S_x^{\rm T}$, a small but non-zero value.

In a real experiment, however, the correlation coefficient is calculated from a limited set of data $\{I_s^{\rm out}(t), \varphi_m^{\rm out}(t)\}$ measured over a finite time $\tau_{\rm ave}$. The thermal correlation coefficient $\mathcal{C}_{\rm T}(\tau_{\rm ave})$ calculated from this data set using Eq. (8) can then reach a non-zero value, of the same order or even larger than the expected quantum correlations $\mathcal{C}_{\rm rad}$. This leads to a constraint on the averaging time $\tau_{\rm ave}$ in order to reach a given accuracy a in the measurement. From the comparison between the dispersion $\Delta\mathcal{C}_{\rm T}(\tau_{\rm ave})$ on the correlations measurement and the expected quantum correlations level $\mathcal{C}_{\rm rad}$, one gets [31]:

$$a = \frac{\Delta\mathcal{C}_{\rm T}(\tau_{\rm ave})}{\mathcal{C}_{\rm rad}} \simeq \sqrt{\frac{S_x^{\rm rad}}{S_x^{\rm T}}} \times \frac{1}{\sqrt{\Gamma_{\rm span}\tau_{\rm ave}}} \tag{9}$$

where $\Gamma_{\rm span}$ is the typical bandwidth of the measurement, namely the spectrum-analyzer bandwidth when working out of the mechanical resonance, or the mechanical bandwidth $\Gamma_{\rm M} = \Omega_{\rm M}/Q$ when the measurement is made at the mechanical resonance frequency.

Working close to a resonance characterized by a high mechanical quality factor, where both the magnitude and the phase of the mechanical behaviour dramatically depend on the frequency, severely expands the averaging time. In contrast, working far enough from any mechanical resonance in order to have a mechanical response as flat in frequency as possible, one has the possibility to integrate the noise over a frequency band as large as possible: with our current setup, one may easily find a 10 kHz-wide frequency band free of any mechanical resonance, to be compared to the 1 Hz or so width of an individual mechanical resonance. For a targeted accuracy of 10%, the expected averaging time for our system at 1 K experiences a 10 000-fold decrease, from 1 hour to less than a second.

Fig. 6 shows an experimental illustration of this time averaging, obtained with a tiny classical intensity noise as in the previous section, with $S_x^{\rm rad}/S_x^{\rm T} \simeq 0.03$. The total correlations $\mathcal{C}_{\rm rad} + \mathcal{C}_{\rm T}$, calculated for 20 different runs (left), clearly tend to

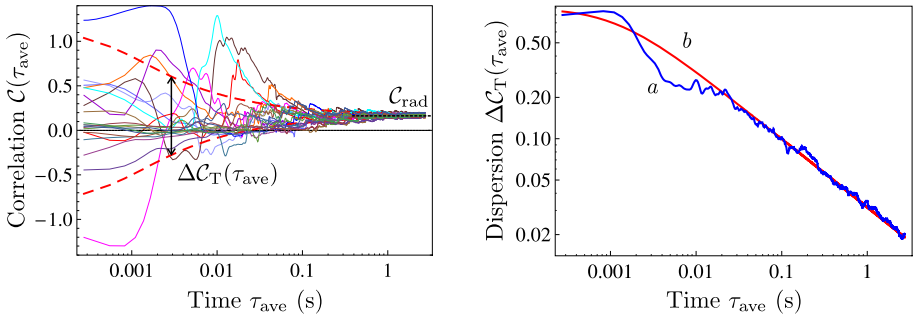

Fig. 6. (Left) Time average of the total correlations $\mathcal{C}_{I_s,\varphi_m} = \mathcal{C}_{rad} + \mathcal{C}_T$, obtained with a classical intensity noise in the $S_x^{rad}/S_x^T \ll 1$ limit. Each curve corresponds to an experimental run, and the dashed curves show the theoretical dispersion $\Delta\mathcal{C}_T(\tau_{ave})$. The correlation tends to its non-zero expected value $\mathcal{C}_{rad}$ within a total average time τ_{ave} shorter than 2 s. (Right) The residual dispersion $\Delta\mathcal{C}_T(\tau_{ave})$ of the correlations is deduced from the experimental runs (a) and compared to a theoretical fit with $\Gamma_{span}/2\pi = 320$ Hz (b), in good agreement with the spectrum-analyzer bandwidth (400 Hz) as experimental and theoretical filter transfer functions do not have the exact same analytical expression.

the expected radiation pressure correlations $\mathcal{C}_{rad} \simeq \sqrt{S_x^{rad}/S_x^T} \simeq 0.17$ after an averaging time of a few seconds. The dispersion $\Delta\mathcal{C}_T$ (right), which characterizes the accuracy a of the measurement, evolves as $1/\sqrt{\tau_{ave}}$ as expected from Eq. (9).

5.2. Contamination of the intensity by displacement noise

Averaging is not the only issue one has to deal with when targeting QRPN with our setup. Since any high-finesse cavity has unavoidable optical losses, a major problem arises from the reflectivity dip at resonance (see Fig. 7). When the laser is not perfectly resonant with the cavity, as the Airy peak slope is non-zero, additional intensity noise stems from displacement noise, which is mainly thermal noise in our case. Neglecting the cavity filtering at the frequency of interest ($\omega_c = \Omega_c/\Omega_{cav} \ll 1$), these additional intensity fluctuations $\delta I_{s,x}^{out}$ are [31]:

$$\delta I_{s,x}^{out} \simeq 4\mathcal{F}\frac{d\bar{I}_s^{out}}{d(\frac{\nu}{\nu_{cav}})}\frac{\delta x_T}{\lambda} \tag{10}$$

as expected from the definition of the slope $d\bar{I}_s^{out}/d\nu$, where $\nu_{cav} = \Omega_{cav}/2\pi$ is the cavity bandwidth, which also corresponds to an equivalent displacement $\lambda/4\mathcal{F}$.

One no longer probes the incident intensity fluctuations responsible for quantum correlations when monitoring the reflected signal intensity, and this inevitably leads to fake correlations as both the signal intensity and meter phase simply display the effect of thermal noise. The thermal correlation coefficient $\mathcal{C}_T(\bar{\nu})$ at a given mean detuning $\bar{\nu}$ (Eq. (8)) no longer vanishes and may become comparable to the quantum correlations $\mathcal{C}_{rad}$, thus limiting the accuracy a of the measurement, now given by [31]:

$$a = \left|\frac{\mathcal{C}_T(\bar{\nu})}{\mathcal{C}_{rad}}\right| \simeq \frac{4\mathcal{F}}{\sqrt{\bar{I}_s^{out}}}\left|\frac{d\bar{I}_s^{out}(\bar{\nu})}{d(\frac{\nu}{\nu_{cav}})}\right|\frac{\sqrt{S_x^T}}{\lambda}\sqrt{\frac{S_x^T}{S_x^{rad}}} \tag{11}$$

This sets a limit upon the maximum mean detuning $\bar{\nu}$ allowed, which only appears in this equation via the slope of the Airy peak $d\bar{I}_s^{out}/d\nu$. Other relevant parameters are the thermal noise amplitude $\sqrt{S_x^T}$, and the ratio $\sqrt{S_x^T/S_x^{rad}}$ between thermal and radiation pressure noises: the accuracy reaches as better values as these 3 parameters are smaller.

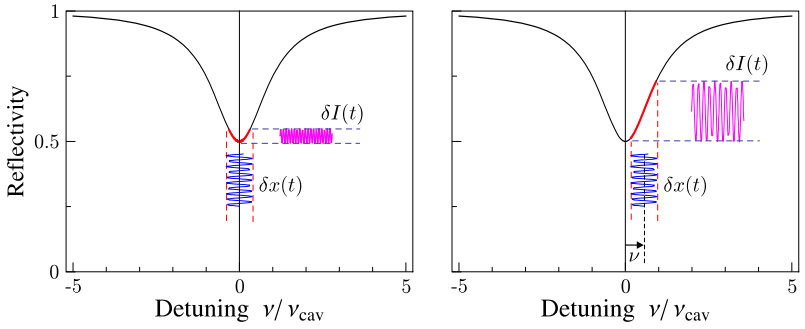

Fig. 7. Principle of the contamination of the reflected intensity of the signal beam by the mirror displacements in a lossy cavity. When the laser frequency is slightly detuned from the cavity resonance (right), the reflected intensity becomes sensitive to mirror displacements.

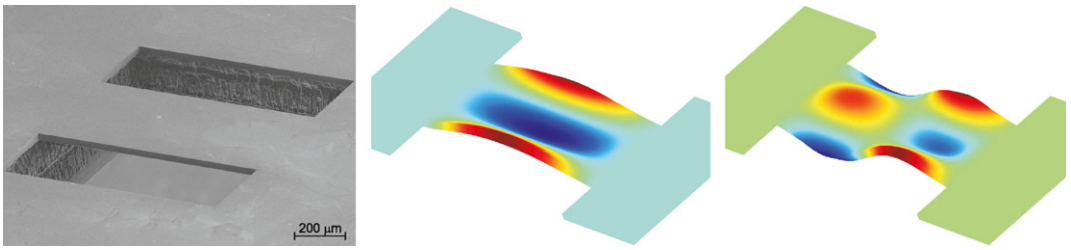

Fig. 8. Silicon beams as optomechanical resonators. Left: SEM view of a 1 mm × 400 μm × 30 μm doubly-clamped beam. Right: Computed vibration profiles of the $(0,2)$ and $(1,2)$ modes.

At the mechanical resonance frequency, where the thermal noise $\sqrt{S_x^{\mathrm{T}}}$ is enhanced by the resonance, this yields:

$$a \simeq \frac{8l}{|1-l|\sqrt{1+l}} \times \frac{k_B T_{\mathrm{m}}}{\hbar \Omega_{\mathrm{M}}} \times \frac{\bar{\nu}}{\nu_{\mathrm{cav}}} \tag{12}$$

where $l = L/T$ is the ratio between the cavity losses L and the transmission T of the front mirror. This equation shows that the requirement on the mean detuning $\bar{\nu}/\nu_{\mathrm{cav}}$ only depends on the cavity losses [first term in (12)], and on the phonon number $k_B T_{\mathrm{m}}/\hbar\Omega_{\mathrm{M}}$ which characterizes the thermal noise level. If one wants to extract optomechanical correlations with a 10% accuracy, for our experimental setup (with $\mathcal{F} = 2\pi/(T+L) = 330\,000$, $L \simeq T/4$), obeying such a relation implies for the frequency mismatch to be lower than 10 mHz (for a 1 MHz cavity bandwidth), which is a very stringent condition.

Lowering the challenge to the stabilization can however be done by working once again far from a resonance frequency. In that case, the thermal noise amplitude $\sqrt{S_x^{\mathrm{T}}}$ in Eq. (11) is indeed much lower and one finds that the maximum frequency mismatch $\bar{\nu}$ is reduced by an amount $1/\phi_0$, where ϕ_0 is the loss angle at the mechanical frequency of interest (for a single resonant mode, one would have $\phi_0 = 1/Q$). With our setup, a value $\phi_0 \simeq 10^{-6}$ yields a frequency locking accuracy that has to be better than 10 kHz, which is quite feasible. Finally note that the same stringent condition on the laser–cavity detuning can be drawn in the regime where radiation pressure noise prevails over thermal noise ($S_x^{\mathrm{rad}} \geqslant S_x^{\mathrm{T}}$) [31].

6. A review of optomechanical systems

We present in this section a review of the different optomechanical resonators under study at Laboratoire Kastler Brossel, with different experimental goals.

6.1. Silicon micro-resonators

As described in Section 4.2, the first optomechanical resonator is a fused silica mirror, which provides both a very high optical finesse and a high mechanical quality factor, at the expense of a rather high mass. Another approach consists in taking advantage of the progress in ion etching of silicon. A typical silicon micromirror (1 mm × 400 μm) doubly-clamped beam, with a thickness of 30 μm allows an optical finesse of the order of 30 000 [12,13], with the following typical optomechanical parameters: $\Omega_{\mathrm{M}}/2\pi \simeq 1$ MHz, $M \simeq 50$ μg, and $Q \simeq 10\,000$ for transverse modes with a low displacement at the clamping location.

One immediately sees that, with the prospect of demonstrating QRPN, the net gain over the mass with respect to the fused silica mirrors (more than 2 orders of magnitude) is lost due to the poorer optical finesse (squared in Eq. (2)) and mechanical quality factor. That specific kind of resonator is currently used in experiments designed to demonstrate 3-mode effects in a nearly degenerate optical cavity [32].

6.2. Quartz micro-pillar

We are also developing a new generation of micromirrors designed for cavity-cooling experiments [13–17], which specifically require a high mechanical resonance frequency in order to reach the resolved sideband regime [17], and a high mechanical quality factor Q as the cooling considerably increases the effective damping of the resonator. To reduce both clamping and coating mechanical losses, our resonator is based on a compression mechanical mode rather than a shear mode: we use the first length extension mode of a quartz micro-pillar, clamped at its center by a thin membrane (see Fig. 9) [33].

Such a mechanical mode is expected to have a very high Q. Single-crystal quartz has been chosen to benefit from its high intrinsic quality factor, especially at low temperature [34,35]. The symmetry of the resonator lowers the displacement at the clamping location, decreasing the clamping losses. Also, the mirror-carrying surface at the top of the pillar has a quasi-null strain, lowering the coating losses. We have used Finite Element Method (FEM) simulations to accurately model the damping, including the real geometry of the resonator and taking into account the etching pattern defects observed after the first microfabrication steps. The size and geometry of both the pillar and the membrane have been carefully optimized

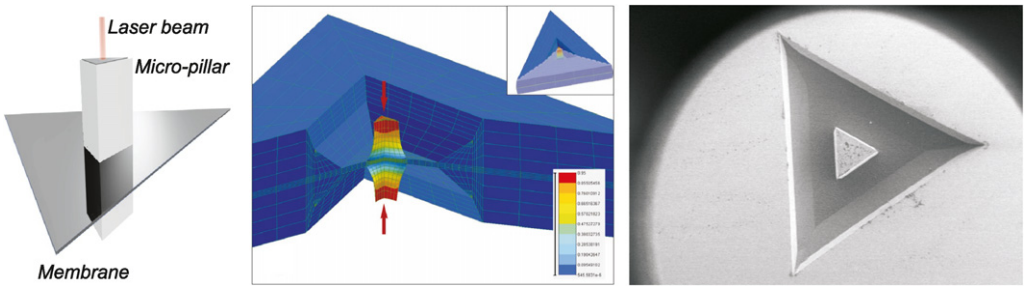

Fig. 9. Quartz micro-pillars as optomechanical resonators. (Left) 3D view of the concept: a symmetrical resonator clamped at the node of its fundamental mode. (Center) FEM simulation of the fundamental mode. (Right) SEM top view of a processed mechanical resonator. The size of the pillar is of the order of 200 μm.

in order to keep the pillar mechanically isolated and to avoid any interference with other mechanical modes. The final processed geometry also respects the quartz internal trigonal symmetry.

Micro-pillars typically have a transverse size of the order of 200 μm and are 1 mm long. The expected mass is then around a few tens of μg. Until now, resonators have been tested without the final optical coating and a test-bench based on a simpler Michelson interferometer configuration has been built to easily measure and optimize the resonator parameters. The current best sample exhibits a very high quality factor, around 400 000 at 0.2 mbar and room temperature, for a resonance frequency of 3.66 MHz. Note that such a system has a radiation-pressure over thermal-noise ratio (2) of a few hundreds at a cryogenic temperature of 100 mK, turning it into a promising candidate to demonstrate QRPN as well.

Such a high Q value can furthermore be considered as an underestimate of the real quality factor since we have not been able to obtain reliable values at lower pressure. The top of the pillar indeed currently has an Au-coating: when the vacuum is better than 10^{-1} mbar, laser light induces a small heating of the mirror surface, which induces a thermal asymmetry of the pillar and a decrease of the quality factor. Such a thermal effect will disappear with the final high-reflectivity coatings.

6.3. Photonic bandgap membrane

A number of theoretical and experimental works have been dedicated to the “membrane-in-the-middle” approach [16], where a thin membrane is inserted inside a high-finesse optical cavity, taking advantage of both the mechanical characteristics of the membrane and the optical properties of the cavity. It has however been shown that the most interesting experiments considered, such as the QND measurement of the number of phonons of the membrane, do require an optical reflectivity very close to unity [16,36]. We study the possibility to use a photonic crystal to fabricate such a high-reflectivity membrane. With a careful choice of the lattice, the photonic crystal can support zero group velocity modes at the so-called Γ point [37]: a normal incidence beam can be fully coupled to in-plane non-propagating resonances, yielding zero transmission. In addition, the dispersion of these modes can be flat enough to have a good reflectivity on a broad range of incidence angles, allowing to work with very small optical waists.

We have started investigating such resonators, to be used as an end mirror in a high-finesse cavity. The resonator is an InP membrane processed by e-beam lithography, with a typical transverse size of a few tens of microns and a thickness of the order of 200 nm. Square holes are processed with a typical step size of 650 nm and a filling factor of 50%.

The mechanical properties of the first membranes have been investigated on our Michelson test-bench. The sample is mounted on a high-frequency/high-power piezoelectric actuator driven by a high power RF amplifier. The spectral response of the membrane is obtained using a network analyzer to synchronously drive the actuator and collect the resulting intensity modulation at the output of the interferometer. Fig. 10 shows the mechanical response of a 10 μm × 20 μm membrane, doubly-clamped by two 1 μm long strips. Observed resonance frequencies are in the MHz band, in excellent agreement with the FEM simulations. The expected masses are of the order of 10 ng. We also note that the frequencies are quite reproducible from one sample to the other, thus emphasizing the quality of the microfabrication process. Mechanical quality factors are currently limited to a few thousands, but may be improved by a better optimization of the geometrical design. Four different loss schemes are identified in such systems: squeeze film damping due to the residual air layer between the membrane and the substrate [38], thermoelastic damping, structural losses due to crystalline defects, and dissipation through the clamping of the resonator to the substrate. The latter has been identified as the very dominant damping mechanism in our case.

From the optical point of view, our Electromagnetic Finite Differences in Time Domain (FDTD) simulations have shown that a careful optimization of the lattice geometry would allow to obtain a high reflectivity over a wide spectral range: theoretical reflectivities can reach more than 99.99% over a spectral window of 30 nm around 1064 nm. We have processed samples of such periodic arrangements of two-dimensional photonic crystal structures and the reflectivity obtained by Fourier Transform InfraRed (FTIR) measurements corroborates some striking spectral features predicted by our simulation. As only uncalibrated reflectivity measurements have been performed yet, work is still underway.

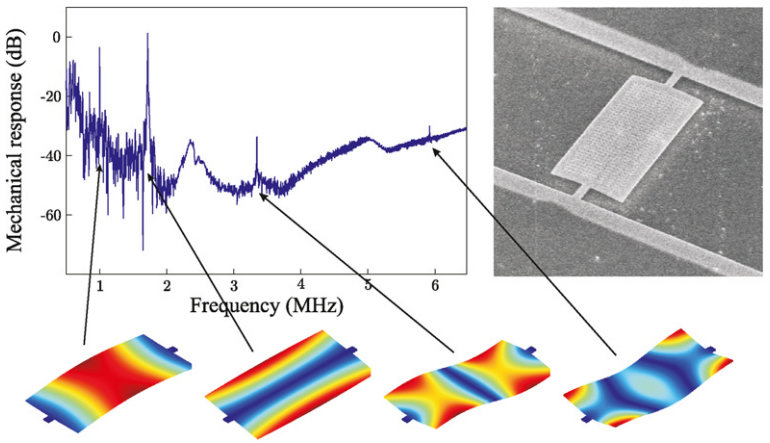

Fig. 10. Photonic crystal membranes as optomechanical resonators. (Left) Mechanical response of an InP membrane, from 500 kHz to 6.5 MHz. Four specific modes are highlighted, together with a FEM simulation of their mode shape. (Right) SEM view of a processed resonator.

7. Conclusion

We have demonstrated optomechanical correlations induced between two light beams by the displacement of a moving mirror through radiation pressure. Although still at the classical level, the technique presented here is extendable to the quantum regime, even in the case where thermal noise is dominant over radiation pressure effects: a temporal average of the experimental signal should enable to retrieve the corresponding quantum correlations and hence demonstrate radiation-pressure noise.

We have theoretically studied the average time needed to detect quantum correlations with a given accuracy, and the effect of the intensity–noise contamination induced by the residual jitter of the laser. Both show that experimental constraints are relaxed when working at a frequency far from any mechanical resonance of the moving mirror: in the case of our plano-convex mirrors, an average time of a few seconds and a jitter less than 10 kHz should be sufficient, whereas the constraints are increased by at least 4 orders of magnitude when working at a mechanical resonance frequency.

Direct observation of quantum radiation pressure noise would benefit from using micromirrors combining very high optical reflectivity and very good mechanical response. For that purpose, we develop new generations of micromirrors. The first one is based on a quartz resonator in a length extension mode. Preliminary experimental measurements give interesting results concerning 3 key parameters of the optomechanical coupling: high resonance frequency, high quality factor and low mass. The second resonator is a photonic-crystal suspended membrane with a size of few tens of microns and a sub-micron thickness. With a careful optimization of the photonic crystal lattice, a high reflectivity for a light beam at normal incidence may be obtained, together with a very low mass.

With a planned ratio between radiation pressure effects and thermal noise expected to be of the order of few hundreds, these new micromirrors are good candidates for the direct observation of quantum radiation pressure effects. One can also envision radiation-pressure-induced quantum optics experiments, such as optomechanical squeezing [39] or QND measurements [23,40].

Acknowledgements

This research was partially funded by the FP7 Specific Targeted Research Projects *Minos* and *QNems*, by the “Agence nationale de la recherche” (ANR) France, Programmes blancs, *ARQOMM* (No. ANR-07-BLAN-2060) and *QuRaG* (No. ANR-09-BLAN-0207), and by the C’Nano Ile de France project *Naomi*.

References

[1] C.M. Caves, Phys. Rev. D 23 (1981) 1693.
[2] M.T. Jaekel, S. Reynaud, Europhys. Lett. 13 (1990) 301.
[3] C. Bradaschia, et al., Nucl. Instrum. Meth. A 289 (1990) 518.
[4] A. Abramovici, et al., Science 256 (1992) 325.
[5] P. Fritschel, Proc. SPIE 4856 (2003) 282.
[6] R.E. Slusher, L.W. Hollberg, B. Yurke, J.C. Mertz, J.F. Valley, Phys. Rev. Lett. 55 (1985) 2409.
[7] K. McKenzie, D.A. Shaddock, D.E. McClelland, B.C. Buchler, P.K. Lam, Phys. Rev. Lett. 88 (2002) 231102.
[8] H. Vahlbruch, et al., Phys. Rev. Lett. 100 (2008) 033602.
[9] Y. Hadjar, P.-F. Cohadon, C.G. Aminoff, M. Pinard, A. Heidmann, Europhys. Lett. 47 (1999) 545.
[10] P.-F. Cohadon, A. Heidmann, M. Pinard, Phys. Rev. Lett. 83 (1999) 3174.
[11] I. Tittonen, et al., Phys. Rev. A 59 (1999) 1038.
[12] O. Arcizet, et al., Phys. Rev. Lett. 97 (2006) 133601.

[13] O. Arcizet, P.-F. Cohadon, T. Briant, M. Pinard, A. Heidmann, Nature (London) 444 (2006) 71.
[14] S. Gigan, et al., Nature (London) 444 (2006) 67.
[15] T. Corbitt, et al., Phys. Rev. Lett. 99 (2007) 160801.
[16] J.D. Thompson, et al., Nature (London) 452 (2008) 72.
[17] A. Schliesser, O. Rivière, G. Anetsberger, O. Arcizet, T.J. Kippenberg, Nature Phys. 4 (2008) 415.
[18] R.G. Knobel, A.N. Cleland, Nature (London) 424 (2003) 291.
[19] M.D. LaHaye, O. Buu, B. Camarota, K.C. Schwab, Science 304 (2004) 74.
[20] A.D. O'Connell, et al., Nature 464 (2010) 697.
[21] K.W. Murch, K.L. Moore, S. Gupta, D.M. Stamper-Kurn, Nature Phys. 4 (2008) 561.
[22] For a review of the current experiments, see the slides of the dedicated session of the 2010 Gravitational-Wave Advanced Detector Workshop, available at http://gw.icrr.u-tokyo.ac.jp/gwadw2010/program/program.html#19-AM.
[23] A. Heidmann, Y. Hadjar, M. Pinard, Appl. Phys. B 64 (1997) 173.
[24] P. Verlot, A. Tavernarakis, T. Briant, P.-F. Cohadon, A. Heidmann, Phys. Rev. Lett. 102 (2009) 103601.
[25] K. Børkje, et al., Phys. Rev. A 82 (2010) 013818.
[26] D. Rugar, R. Budakian, H.J. Mamin, B.W. Chui, Nature (London) 430 (2004) 329.
[27] T. Caniard, P. Verlot, T. Briant, P.-F. Cohadon, A. Heidmann, Phys. Rev. Lett. 99 (2007) 110801.
[28] C.M. Mow-Lowry, B.S. Sheard, M.B. Gray, D.E. McClelland, S.E. Whitcomb, Phys. Rev. Lett. 92 (2004) 161102.
[29] T. Briant, P.-F. Cohadon, A. Heidmann, M. Pinard, Phys. Rev. A 68 (2003) 033823.
[30] T. Briant, P.-F. Cohadon, M. Pinard, A. Heidmann, Eur. Phys. J. D 22 (2003) 131.
[31] P. Verlot, A. Tavernarakis, T. Briant, P.-F. Cohadon, A. Heidmann, in preparation.
[32] C. Zhao, L. Ju, H. Miao, S. Gras, Y. Fan, D.G. Blair, Phys. Rev. Lett. 102 (2009) 243902.
[33] M. Bahriz, et al., IEEE Conf. on Sensors, 2010, accepted for publication.
[34] O. Arcizet, R. Rivière, A. Schliesser, G. Anetsberger, T.J. Kippenberg, Phys. Rev. A 80 (2009) 021803.
[35] A. Schroeter, et al., arXiv:0709.4359.
[36] A.M. Jayich, et al., New J. Phys. 10 (2008) 095008.
[37] F. Raineri, et al., Appl. Phys. Lett. 86 (2005) 011116.
[38] H. Sumali, J. Micromech. Microeng. 17 (2007) 2231.
[39] C. Fabre, et al., Phys. Rev. A 49 (1994) 1337.
[40] K. Jacobs, P. Tombesi, M.J. Collett, D.F. Walls, Phys. Rev. A 49 (1994) 1961.